

1 **Atmospheric dynamics of IR-active particles released from Mars' surface.**

2

3 Mark I. Richardson^{1,*}, Samaneh Ansari², Bowen Fan^{3,4}, Ramses Ramirez⁵, Hooman Mohseni²,
4 Michael A. Mischna⁶, Michael H. Hecht⁷, Liam J. Steele^{3,8}, Felix Sharipov⁹, Edwin S. Kite^{3,*}

5

6 1. Aeolis Research, Chandler, AZ.

7 2. Northwestern University, Evanston, IL.

8 3. University of Chicago, Chicago, IL.

9 4. Now at: Yale University, New Haven, CT.

10 5. University of Central Florida, Orlando, FL.

11 6. Jet Propulsion Laboratory, California Institute of Technology, Pasadena, CA.

12 7. MIT Haystack Observatory, Westford, MA.

13 8. Now at: European Center for Medium-Range Weather Forecasts, Reading, UK.

14 9. Universidade Federal do Paraná, Curitiba, Paraná, Brazil.

15 *Corresponding authors, mir@aeolisresearch.com and kite@uchicago.edu

16

17 **Key points:**

- 18 • Using a plume-tracking climate model, we investigate radiative-dynamical feedback from
19 release of two particle compositions at Mars' surface.
- 20 • For a single, constant source, global particle abundance saturates in no more than 4 Mars
21 Years, enabling Mars surface and atmospheric warming.
- 22 • Self-lofting helps particles rise and spread, and an enhanced Hadley cell aids global mixing.

23 **Plain language summary.**

24 Both aerosols and gases have been proposed as ways of warming Mars. For the aerosol method,
25 particles released locally must disperse globally. We address this question for the first time using
26 a plume-tracking, dry Martian global atmospheric model. We find that for a single, constant source,
27 global particle abundance saturates in <4 Mars Years, enabling Mars surface and atmospheric
28 warming. Self-lofting helps particles rise and spread, and stronger winds help global mixing.
29 Warming is strong, but varies depending on model set-up (stronger in 3-D models than in 1-D
30 models). Many open atmospheric science questions remain, including the role of agglomeration,
31 dry-deposition rate uncertainty, and modeling water cycle feedbacks.

32

33 **Abstract.**

34 Surface release of radiatively active particles, with high infrared- (IR-)to-visible extinction ratios,
35 has been proposed as a method of warming Mars. However, to warm Mars using aerosols, particles
36 released locally must disperse globally. Here we provide an initial reference study in a plume
37 tracking, dry Martian atmospheric model to address this question. The winds that transport aerosols
38 respond to the aerosol's IR forcing, implying strong radiative-dynamical feedbacks (RDF). We
39 investigate RDF from surface release of two particle compositions: carbon (graphene) and metal
40 (Al). Self-lofting helps particles rise and spread locally and regionally, and the Hadley cell
41 strengthens under warming, aiding latitudinal mixing. Within our model, Mars RDF enable
42 engineered-aerosol warming. Warming is slightly greater for three-dimensional vs. 1D-models and
43 also depends on spectral resolution of radiative transfer. We assess implications for Mars warming.
44 Many open atmospheric science questions remain, including the role of agglomeration, dry-
45 deposition rate uncertainty, and modeling water cycle feedbacks.

46

47 **1. Introduction.**

48 Mars is a cold desert, with a weak greenhouse effect (+5 K from its 6 mbar CO₂ atmosphere),
49 abundant frozen H₂O (Carr & Head 2015), and 7-100 mbar of sequestered volatilizable CO₂
50 (Bierson et al. 2016, Buhler & Piqueux 2020). It has been debated for decades whether or not
51 humans should warm Mars for the purposes of human habitation, with arguments both for (McKay
52 1990) and against (Marshall 1993). If we decide in the future to modify Mars' environment (Sagan
53 1973), there is consensus that warming Mars by >30 K would be needed for seasonal meltwater

54 (e.g., Avernier et al. 1976, McKay et al. 1991, Pollack & Sagan 1993, Graham 2004, Marinova et al.
55 2005); an up-to-date review is DeBenedictis et al. (2025). While such warming long seemed
56 impractical (Jakosky & Edwards 2018), recent developments suggest new Mars-warming methods
57 (e.g., Wordsworth et al. 2019), including release of IR-active particles (Ansari et al. 2024).
58 However, prior work on warming with IR-active particles assumed static aerosol distributions
59 based on natural dust aerosol distribution (Ansari et al. 2024) rather than modeling the dynamical
60 behavior of engineered aerosol.

61 Aerosols are an important radiative agent in planetary atmospheres (Yung & DeMore 1999,
62 Kahre et al. 2017). Previous studies have examined aerosol feedbacks on Mars for natural particles,
63 from local "solar escalator" effects (Spiga et al. 2013, Daerden et al. 2015, Batterson et al. 2023)
64 to larger scales (e.g., Murphy et al., 1993, Wilson and Hamilton, 1996, Newman et al., 2002,
65 Rafkin 2009, Kahre et al. 2015, Gebhardt et al. 2021, Urata et al. 2025) and on Earth for smoke,
66 volcanic ash, and other applications (De Laat et al. 2012, Yu et al. 2019, Khaykin et al. 2020,
67 Visioni et al. 2020, Gao et al. 2021, Ohneiser et al. 2023). However, the engineered aerosols
68 considered for warming Mars have (by design) much stronger interaction with thermal-IR
69 emission than with sunlight, whereas previous work has focused on self-lofting driven by
70 absorption of sunlight. Ansari et al. (2024) considered IR-active particles but assumed a static
71 particle distribution. Given that RDF will be strong for IR-active particles released from Mars'
72 surface, key atmospheric-dynamics questions remain: How high are aerosols lofted? How widely
73 do they disperse? How do they couple with atmospheric circulation locally and globally? How
74 long until steady state is reached? Does release location matter? Any Mars-warming method would
75 face problems of manufacturing and environmental impact (e.g., both potential impact on humans
76 and/or introduced plant life, and on, e.g., planetary climate via albedo changes) as well, but the
77 radiative-dynamical questions must be addressed first. To this end, we added radiatively active
78 engineered nanoparticle tracking to the Mars Weather Research and Forecasting (MarsWRF) code
79 (Richardson et al. 2007, Toigo et al. 2012), building on previous work tracking methane plumes
80 (Mischna et al. 2011, Luo et al. 2021) (Methods). We specifically focus in this initial study on the
81 simplest case of non-coagulating particles in a dry atmosphere released from a single, continuous
82 source. This is done to minimize process complexity for this initial study and is not due to
83 limitations with the model. More complex modeling will be necessary in the future to more
84 completely address realistic release scenarios, particulate microphysical behavior, and climate

85 physics. Instead, this study provides the necessary next step from idealized and/or 1D work that
86 has been undertaken so far and provides a reference baseline for interpretation of future, more
87 complex simulations.

88

89 **2. Methods.**

90 We carry out separate numerical experiments that each consider one of two particle types for Mars
91 warming: carbon (graphene disks) and metal (Al rods). Both target Mars' thermal infrared (TIR)
92 windows at $\sim 10\ \mu\text{m}$ and $\sim 20\ \mu\text{m}$ via different mechanisms. Few-hundred-nm diameter graphene
93 disks resonantly absorb TIR (Fang et al. 2014). To cover both spectral windows (Fig. S3), in the
94 graphene trials we used 16 parts (by number) 250 nm diameter disks to one part 1000 nm diameter
95 disks. Graphene is translucent to visible light, though it requires potentially costly modification
96 for optimal performance (Supporting Information). Here, we adjust the electronic properties of the
97 simulated graphene to give resonance height and width similar to Al rods. This implicitly assumes
98 graphene is modified ("doped") to increase the carrier concentration (Supporting Information).
99 The Al rods (60 nm-diameter, 8 μm long, one-eighth the weight of the particles considered in
100 Ansari et al. 2024) both absorb and scatter thermal IR (Forget & Pierrehumbert 1997). Either or
101 both particle types might require anti-stick coatings, which are not modeled here. The goal is to
102 examine plausible particles that might be produced: the chosen particles are not optimized for
103 warming. As such, this study yields potentially realistic heating. It does not represent an upper
104 limit on heating.

105 In our 3D (MarsWRF) modeling, we simulated continuous near-surface release of IR-
106 active particles at both a northern-hemisphere midlatitude site (202°E 40°N, Arcadia Planitia), and
107 separately at an equatorial site (135°E 0°N, Elysium Planitia), expressing release rate in
108 liters/second (L/s) of solid aerosol (ranging from 0-60 L/s, Table S3). Particles can settle at the
109 surface and we do not include any re-lofting mechanism. For natural dust, we imposed a time-
110 varying background of radiatively active natural dust derived from an observational database
111 (Montabone et al. 2015) for Mars Year 30, corresponding to a relatively storm-free scenario. The
112 vertical distribution was further adjusted to that observed by Mars Climate Sounder (Kleinböhl et
113 al., 2024). Dust was not allowed to interact with the engineered particles. Particle agglomeration
114 is not included in the model, which is a significant limitation (Discussion). Gravitational settling
115 speeds are obtained from analytical free molecular calculations for the appropriate shapes

116 (Supporting Information). We also set the dry deposition velocity in the lowermost model layer,
117 which is ~ 9 m thick, to a minimum of 0.03 cm/s, to represent the effect of diffusive removal of
118 small particles (Supporting Information). For comparison, the empirical exponential decay
119 timescale for natural dust optical depth is ~ 50 sols (Kahre et al. 2017).

120 We also used a 1D radiative-convective equilibrium model with Mars-average insolation
121 (e.g., Ramirez 2017) and a Single Column Model (SCM) version of WRF as a cross-check on
122 warming. Results are shown in Figs. S14-S15 and Table S4. The warming in 1D and 3D models
123 differ (as do baseline global temperatures with no nanoparticle opacity), even when the same
124 radiative transfer scheme is used (WRF SCM vs. GCM). The differences can be traced to
125 differences in the vertical temperature profiles (and specifically temperature assumptions at the
126 tropopause), the spectral resolution for radiative transfer, and the treatment of the atmosphere as a
127 3D system (see Supplementary Materials).

128

129 **3. Results.**

130 High-spatial-resolution simulations show RDF during the initial release of IR-active particles in a
131 nested version of MarsWRF. Fig. 1 shows results for release from the midlatitude site for 60 nm
132 diameter Al rods at a rate of 60 L/s. The plume self-lofts and thickens the Planetary Boundary
133 Layer (PBL) height (Fig. 1a,b show column visible opacity and PBL height at 11AM local time at
134 the release site), which is $\sim 2\times$ thicker than without self-lofting (Fig. S7). Above the release point
135 (Fig. 1c, top row), particles accumulate in the nighttime PBL before mixing upward during
136 daytime. In adjacent grid boxes (Fig. 1c, middle row), particles mix across the surface layer during
137 late night and predawn, while early evening winds leave this region particle-free. Several grid
138 points downwind (Fig. 1c, bottom row), a detached high "anvil" of particles dominates the
139 nanoparticle mass mixing ratio (mmr) between 5 and 10 km above the surface. Further from the
140 plume (Fig S7), the particle mmr peaks between about 7.5 and 12.5 km, at or above the top of the
141 plume-free PBL. The vertical distribution of particles evolves as follows. While initially depleted
142 at altitude, within 100 days an aerosol-enriched layer forms above 7 km. During southern spring,
143 the strong Hadley cell temporarily halts particle buildup (Fig. S6). These vertical variations
144 diminish to 10% over years as mixing homogenizes the atmosphere. The steady-state particle
145 distribution shows only a modest longitudinal enhancement (15° full-width-at-half-maximum)

146 centered on the release site. Particle optical depth in steady state varies seasonally by 15-20%,
147 rising during northern summer when winds are weakest, regardless of release location.

148 Fig. 2a-f shows the global spread of nanoparticle mmr in lower resolution simulations
149 ($5^\circ \times 5^\circ$), for release at an equatorial site. The lower resolution is used to allow many more
150 simulations to be undertaken than is possible for nested cases (such as for Fig. 1). The high
151 resolution allows more detail to be seen in the plume distribution but does not change the main
152 results. The warming plume spreads eastward at all altitudes and also westward at high altitude in
153 the high latitudes, with inter-hemispheric mixing occurring within months. These particles achieve
154 warming much more efficiently than previous designs—a visible optical depth (τ_{vis}) of 0.2 requires
155 only $\sim 45 \text{ mg/m}^2$ of aluminum rods in the aluminum simulations, and the same optical depth
156 requires just over $\sim 17.5 \text{ mg/m}^2$ of graphene in the graphene simulations. The particles are more
157 than twice as radiatively effective (in the thermal IR, per unit mass) than previous designs. The
158 warming atmosphere inflates both in the sense of vertical expansion due directly to increased scale
159 height, but also due to reduction in total mass of the seasonal CO_2 ice caps, see Table S3. This
160 inflation combined with the RDF self-lofting lifts the suspended particles high into the atmosphere.
161 The system approaches steady state with an e-folding timescale of ~ 1.1 Mars years (Fig. 3, Fig.
162 S8). The total time to achieve warming is about the same as the particle atmospheric lifetime.
163 Cooling after particle release ends follows the same timescale. This timescale emerges from the
164 model as the timescale for mixing any aerosol with similar radiative properties. Nothing has been
165 done to make the particles mix more rapidly.

166 Fig. 2d shows warm season surface temperatures. The warm season surface temperature is
167 defined as the average surface temperature during the warmest 36° of solar longitude (~ 70 days)
168 of the year. This corresponds to southern summer in the southern ground ice zone, and northern
169 summer in the northern ground ice zone.

170 The warmed climate develops a stronger meridional overturning circulation (Fig. 4). The
171 Hadley cells strengthen by a factor of 4 and shift upwards while the seasonal strength asymmetry
172 (Richardson & Wilson 2002) largely disappears. Because the particles are relatively well mixed in
173 steady state, the mass streamfunction corresponds to the meridional overturning circulation of
174 particles. Near-surface winds increase by 60% (global and annual average). Steeper temperature
175 gradients develop between sunlit regions and the winter pole. This is the opposite of Earth's CO_2 -
176 warming response, which preferentially warms the poles and weakens circulation (Xia et al. 2020).

177 Surface pressure increases as seasonal CO₂ seasonal ice caps shrink. We do not consider
178 release of additional CO₂ from perennial CO₂ ice nor from adsorbed regolith reservoirs, which
179 would at least double the atmospheric pressure under warming (Bierson et al. 2016, Buhler &
180 Piqueux 2020). This thicker CO₂ atmosphere would add to the greenhouse effect, moderate the
181 equator-pole temperature gradient, and expand the percentage of surface area above the triple point
182 of water (Dickson et al. 2023).

183 The IR-active aerosols spread broadly, unlike patchy dust storms on Earth and Mars,
184 because they settle very slowly. When artificially ballasted to give a settling speed corresponding
185 to the diameter of natural Mars dust (3 μm), the particles produce strong concentration gradients—
186 column depth varies by 5× between the release latitude and south pole, and particles remain below
187 200 Pa altitude. This creates localized warming, with a 2000 km-wide +10 K warming zone,
188 though less efficiently than global warming.

189 Among the two release sites tested, steady-state temperature is modestly warmer for
190 equatorial release (Fig. S9), with greater temperature differences for higher particle loads. The
191 steady-state particle loading is also slightly higher, as expected given the longer distances (and
192 correspondingly longer time for sedimentation) for particles released from a far northern site to
193 spread globally.

194 **4. Discussion.**

195 For the first time, we modeled the atmospheric dynamics of IR-active particles released from Mars'
196 surface in a global 3D model. Further research is needed on both Mars and warming options before
197 committing to any plan for Mars' future (DeBenedictis et al. 2025). For example, the case for
198 maintaining Mars' surface as a pristine wilderness indefinitely is given in Marshall (1993).
199 Moreover, making Mars' surface suitable for life involves many steps beyond initial warming, for
200 example, soil chemistry and suitability for biology (DeBenedictis et al. 2025). Progress here would
201 be useful for both investigations of Mars' possible future habitability and for astrobiology research
202 (Wordsworth & Cockell 2024, Wordsworth et al. 2025).

203 As warmer climates have more water vapor, and water vapor is a greenhouse gas, water
204 vapor feedback will strengthen warming. Water ice clouds have also been proposed to provide
205 strong positive feedback for Mars warming (*e.g.*, Wilson et al, 2008, Madeleine et al. 2014),
206 although this depends on grain size and cloud height. As the water cycle intensifies, aerosol may
207 act as ice nuclei / cloud condensation nuclei, which may scavenge aerosol. Even if snow does not

208 reach the ground, scavenging can still transport aerosol vertically downward prior to sublimation
209 (i.e., virga). These examples show that water cycle feedbacks require further study. Additionally,
210 a more active water cycle within a circulation that has enhanced “dust storm-like” global
211 circulation (Fig.4d) will likely greatly increase water atmospheric loss rates to space (Heavens et
212 al. 2018, Chaffin et al. 2021) above the current rate of approximately 0.005% of Mars' confirmed
213 water inventory per million years.

214 Several unmodeled dust feedbacks are potentially important. Initially, stronger surface
215 winds would lift more dust (Hartwick et al. 2022), creating a potential negative feedback since
216 dust reduces dayside temperatures despite causing net warming (Streeter et al. 2020). However,
217 strong warming would eliminate the CO₂ ice cap edge where strong dust lifting generates most
218 Martian dust storms (Kahre et al. 2017). Additionally, dust can be trapped both by surface liquid
219 water and in high-altitude 'duststones' (Bridges & Muhs 2012).

220 Aerosol-aerosol and aerosol-surface interactions warrant further research. Agglomeration
221 of particles (Bertrand et al. 2022) is most likely during dispersal. Scavenging by condensation of
222 water onto the engineered aerosol could remove a significant fraction of the particles. Possible
223 mitigations include anti-stick coatings, more dispersal points, charging, and day-only release.
224 Since coatings can be very thin (atomic scale), they need not matter much for radiative properties.
225 Agglomerates are deliberately produced during aerosol synthesis (and their properties tuned)
226 (Friedlander 2000, Buesser & Pratsinis 2012), and it is possible that agglomerates will remain both
227 efficient at Mars warming and also easily wind-transported, depending on their fractal dimension.
228 Agglomeration between engineered aerosols and natural dust might also occur. Few data exist
229 regarding dry deposition of submicron particles on desert surfaces, and this uncertainty is
230 important (e.g., Zhang & Shao 2014, Emerson et al. 2020, Li et al. 2025). If the dry deposition rate
231 is 3× greater, then the particle lifetime will be 3× shorter for slow-settling particles such as
232 graphene disks.

233 Particles must be engineered to break down in the natural environment. Methods include
234 adding spacers, designing for water solubility, further thinning for oxidation frangibility, and
235 functionalization. Graphene particles could offer additional benefits if doped with soil nutrients.

236 In our simulations, even though Mars' low-latitude temperature swings are reduced, they
237 remain ~100 K, and winter-minimum temperatures in the ground-ice-rich latitudes remain cold

238 (<230 K for latitudes poleward of 30°). These swings will moderate as Mars' atmospheric thickness
239 further increases but will remain severe by Earth standards.

240 Other particle release strategies might lead to stronger warming than the continuous and
241 steady one used here. For example, particles could be released during the season when the
242 circulation at the site is upward, or at locations and times that have strong diurnal updrafts.

243 We note that although self-lofting helps particles rise and spread for initial deployment
244 (Fig. 1 and Fig. S7), and we run to steady state, we have not determined whether the self-lofting
245 is important in maintaining, as opposed to establishing, the steady-state warmed atmosphere.

246 Either carbon or metal particles could warm Mars from near-surface release, if produced
247 at scale. The details of how particles are prepared with both high throughput and sufficient
248 uniformity are challenging (Supporting Information).

249 Analyzing Mars with stronger longwave forcing but the same orbital forcing
250 is scientifically interesting, especially as comparison to Mars' geologically recent past, with similar
251 longwave forcing but different orbital forcing, is a major scientific goal (MEPAG 2025).

252

253 **5. Conclusions.**

254 Using a particle-tracking climate model, we simulated the atmospheric dynamics of warming Mars
255 with engineered aerosol. We find that radiative-dynamical feedbacks, including local self-lofting
256 and stronger large-scale circulation, aids particle spread. This study addresses only some aspects
257 of the question of IR-active particle release might modify Mars' climate: atmospheric processes
258 are inherently complex, and many open questions remain. These include water cycle feedbacks
259 and agglomeration mitigation approaches.

260 **Acknowledgements.** We thank C. Willard, A.S. Braude, M. Wang, M. Hersam, R. Zubrin,
261 N. Myrhvold, D. Keith, C. Lee, A.P. Raman, M. Mester, and the PlanetWRF development team.
262 This work used GrADS (COLA/IGES). This work used resources from the University of Chicago's
263 Research Computing Center. Part of the resources supporting this work were provided by the
264 NASA High-End Computing (HEC) Program through the NASA Advanced Supercomputing
265 (NAS) Division at Ames Research Center. This research was supported in part through the
266 computational resources and staff contributions provided for the Quest high performance
267 computing facility at Northwestern University which is jointly supported by the Office of the
268 Provost, the Office for Research, and Northwestern University Information Technology. A portion

269 of this work was conducted at the Jet Propulsion Laboratory, California Institute of Technology,
270 under a contract with NASA.

271
272 **Open research / data availability statement.** Model output corresponding to the figures shown
273 is available, see Richardson & Kite (2025). FDTD: 3D Electromagnetic Simulator is commercial
274 code (Lumerical). The MarsWRF source code can be made available by Aeolis Research pending
275 scientific review and a completed Rules of the Road agreement. Requests for the MarsWRF source
276 code should be submitted to mir@aeolisresearch.com.

277
278 **Conflict of interest statement.** The authors declare there are no conflicts of interest for this
279 manuscript.

280
281 **References.**

282 Ansari, S., Kite, E.S., Ramirez, R., Steele, L.J. and Mohseni, H., 2024. Feasibility of keeping Mars warm
283 with nanoparticles. *Science Advances*, 10(32), p.eadn4650. <https://doi.org/10.1126/sciadv.adn4650>

284 Averner, M.M. and MacElroy, R.D., 1976. On the habitability of Mars: An approach to planetary
285 ecosynthesis (NASA-SP-414).

286 Batterson, C.M., Kahre, M.A., Bridger, A.F., Wilson, R.J., Urata, R.A. and Bertrand, T., 2023. Modeling
287 the “B” regional dust storm on Mars: Dust lofting mechanisms predicted by the new NASA Ames Mars
288 GCM. *Icarus*, 400, p.115542. <https://doi.org/10.1016/j.icarus.2023.115542>

289 Bierson, C.J., Phillips, R.J., Smith, I.B., Wood, S.E. Putzig, N.E., Nunes, D., and Byrne, S., 2016.
290 Stratigraphy and evolution of the buried CO₂ deposit in the Martian south polar cap. *Geophys. Res. Lett.*
291 43, 9, 4172-4179. <https://doi.org/10.1002/2016GL068457>

292 Bridges, N.T. and Muhs, D.R., 2012. Duststones on Mars: Source, transport, deposition, and erosion, in
293 Grotzinger & Milliken, *Sedimentary Geology of Mars*, SEPM Special Publication 102.

294 Buesser, B. and Pratsinis, S.E., 2012. Design of nanomaterial synthesis by aerosol processes. *Annual*
295 *Review of Chemical and Biomolecular Engineering*, 3(1), pp.103-127. <https://doi.org/10.1146/annurev-chembioeng-062011-080930>

297 Buhler, P.B. and Piqueux, S., 2021. Obliquity-driven CO₂ exchange between Mars' atmosphere, regolith,
298 and polar cap. *J. Geophys. Res.: Planets*, 126(5), p.e2020JE006759. <https://doi.org/10.1029/2020JE006759>

- 299 Carr, M.H., and Head, J.W. (2015). Martian surface/near-surface water inventory: Sources, sinks, and
 300 changes with time. *Geophys. Res. Lett.*, 42(3), 726--732. <https://doi.org/10.1002/2014GL062464>
- 301 Chaffin, M.S., Kass, D.M., Aoki, S. et al., 2021. Martian water loss to space enhanced by regional dust
 302 storms. *Nat Astron* 5, 1036–1042. <https://doi.org/10.1038/s41550-021-01425-w>
- 303 Daerden, F., Whiteway, J.A., Neary, L., Komguem, L., Lemmon, M.T., Heavens, N.G., Cantor, B.A.,
 304 Hébrard, E. and Smith, M.D., 2015. A solar escalator on Mars: Self-lifting of dust layers by radiative
 305 heating. *Geophys. Res. Lett.*, 42(18), pp.7319-7326. <https://doi.org/10.1002/2015GL064892>
- 306 De Laat, A.T.J., Stein Zweers, D.C., Boers, R. and Tuinder, O.N., 2012. A solar escalator: Observational
 307 evidence of the self-lifting of smoke and aerosols by absorption of solar radiation in the February 2009
 308 Australian Black Saturday plume. *J. Geophys. Res.: Atmospheres*, 117(D4).
 309 <https://doi.org/10.1029/2011JD017016>
- 310 DeBenedictis, E.A., Kite, E.S., Wordsworth, R.D., Lanza, N.L., Cockell, C.S., Silver, P.A., Ramirez, R.M.,
 311 Cumbers, J., Mohseni, H., Mason, C.E., Fischer, W.W., & McKay, C.P., The case for Mars terraforming
 312 research, <https://doi.org/10.1038/s41550-025-02548-0>, *Nature Astronomy*, 2025.
- 313 Dickson, J.L., Palumbo, A.M., Head, J.W., Kerber, L., Fassett, C.I. and Kreslavsky, M.A., 2023. Gullies
 314 on Mars could have formed by melting of water ice during periods of high obliquity. *Science*, 380(6652),
 315 pp.1363-1367. <https://doi.org/10.1126/science.abk2464>
- 316 Emerson, E.W., Hodshire, A.L., DeBolt, H.M., Bilsback, K.R., Pierce, J.R., McMeeking, G.R. and Farmer,
 317 D.K., 2020. Revisiting particle dry deposition and its role in radiative effect estimates. *Proceedings of the*
 318 *National Academy of Sciences*, 117(42), pp.26076-26082.
- 319 Fang, Z., Thongrattanasiri, S., Schlather, A., Liu, Z., Ma, L., Wang, Y., Ajayan, P.M., Nordlander, P.,
 320 Halas, N.J. and García de Abajo, F.J., 2013. Gated tunability and hybridization of localized plasmons in
 321 nanostructured graphene. *ACS Nano*, 7(3), pp.2388-2395. <https://doi.org/10.1021/nn3055835>
- 322 Fang, Z., Wang, Y., Schlather, A.E., Liu, Z., Ajayan, P.M., García de Abajo, F.J., Nordlander, P., Zhu, X.
 323 and Halas, N.J., 2014. Active tunable absorption enhancement with graphene nanodisk arrays. *Nano*
 324 *Letters*, 14(1), 299-304. <https://doi.org/10.1021/nl404042h>
- 325 Feldman, W.C., Prettyman, T.H., Maurice, S. et al., 2004. Global distribution of near-surface hydrogen on
 326 Mars, *J. Geophys. Res.* 109, E09006.
- 327 Friedlander, S.K., 2000. *Smoke, dust, and haze*, 2nd Edition. New York: Oxford University Press.
- 328 Forget, F. and Pierrehumbert, R.T., at1997. Warming early Mars with carbon dioxide clouds that scatter
 329 infrared radiation. *Science*, 278(5341), pp.1273-1276. <https://doi.org/10.1126/science.278.5341.1273>

- 330 Gao, R.S., Rosenlof, K.H., Kärcher, B., Tilmes, S., Toon, O.B., Maloney, C. and Yu, P., 2021. Toward
 331 practical stratospheric aerosol albedo modification: Solar-powered lofting. *Science Advances*, 7(20),
 332 p.eabe3416. <https://doi.org/10.1126/sciadv.abe3416>
- 333 Gebhardt, C., Abuelgasim, A., Fonseca, R.M., Martín-Torres, J. and Zorzano, M.P., 2021. Characterizing
 334 dust-radiation feedback and refining the horizontal resolution of the MarsWRF model down to 0.5 degree.
 335 *J. Geophys. Res.: Planets*, 126(3), p.e2020JE006672. <https://doi.org/10.1029/2020JE006672>
- 336 Graham, J.M., 2004. The biological terraforming of Mars: Planetary ecosynthesis as ecological succession
 337 on a global scale. *Astrobiology*, 4(2), pp.168-195. <https://doi.org/10.1089/153110704323175133>
- 338 Hartwick, V.L., Haberle, R.M., Kahre, M.A. and Wilson, R.J., 2022. The dust cycle on Mars at different
 339 orbital distances from the Sun: An investigation of the impact of radiatively active dust on land planet
 340 climate. *The Astrophysical Journal*, 941(1), p.54.
- 341 Heavens, N.G., Kleinböhl, A., Chaffin, M.S. et al., 2018. Hydrogen escape from Mars enhanced by deep
 342 convection in dust storms. *Nat. Astron.* 2, 126–132. <https://doi.org/10.1038/s41550-017-0353-4>
- 343 Jakosky, B.M. and Edwards, C.S., 2018. Inventory of CO₂ available for terraforming Mars. *Nature*
 344 *Astronomy*, 2(8), pp.634-639.
- 345 Kahre, M.A., Hollingsworth, J.L., Haberle, R.M. and Wilson, R.J., 2015. Coupling the Mars dust and water
 346 cycles: The importance of radiative-dynamic feedbacks during northern hemisphere summer. *Icarus*, 260,
 347 pp.477-480. <https://doi.org/10.1016/j.icarus.2014.07.017>
- 348 Kahre, M.A., Murphy, J.R., Newman, C.E., Wilson, R.J., Cantor, B.A., Lemmon, M.T., Wolff, M.J., "The
 349 Mars dust cycle" in *The Atmosphere and Climate of Mars*, R. Haberle, R. T. Clancy, F. Forget, M. D. Smith,
 350 and R. W. Zurek, Eds. (Cambridge Univ. Press, 2017), pp. 295.
- 351 Khaykin, S., Legras, B., Bucci, S., Sellitto, P., Isaksen, L., Tencé, F., Bekki, S., Bourassa, A., Rieger, L.,
 352 Zawada, D. and Jumelet, J., 2020. The 2019/20 Australian wildfires generated a persistent smoke-charged
 353 vortex rising up to 35 km altitude. *Communications Earth & Environment*, 1(1), p.22.
 354 <https://doi.org/10.1038/s43247-020-00022-5> |
- 355 Kleinböhl, A., Kass, D.M., Schreier, M., Piqueux, S., Suzuki, S., Shirley, J.H., Chen, L., and Schofield,
 356 J.T., 2024. Far infrared radiative properties of Mars atmospheric aerosols and their application to Mars
 357 Climate Sounder retrievals of aerosol profiles, aerosol columns and surface temperatures. *Icarus* 419,
 358 116000. <https://doi.org/10.1016/j.icarus.2024.116000>
- 359 Li, L., Zhao, C., Newman, C.E., Zhao, Y., Feng, J., Li, T., Yang, C. and Yue, Y., 2025. Impacts of dry
 360 deposition processes with resolved dust particle sizes on simulating the Martian dust. *J. Geophys. Res.:*
 361 *Planets*, 130(5), p.e2024JE008616. <https://doi.org/10.1029/2024JE008616>

- 362 Luo, Y., Mischna, M.A., Lin, J.C., Fasoli, B., Cai, X. and Yung, Y.L., 2021. Mars methane sources in
363 northwestern Gale crater inferred from back trajectory modeling. *Earth and Space Science*, 8(11),
364 p.e2021EA001915. <https://doi.org/10.1029/2021EA001915>
- 365 Marinova, M.M., McKay, C.P. and Hashimoto, H., 2005. Radiative-convective model of warming Mars
366 with artificial greenhouse gases. *J. Geophys. Res.: Planets*, 110(E3). <https://doi.org/10.1029/2004JE002306>
- 367 Marshall, A., 1993. Ethics and the extraterrestrial environment. *Journal of Applied Philosophy*, 10, 227-
368 236.
- 369 McKay, C.P., 1990, Does Mars have rights? An approach to the environmental ethics of planetary
370 engineering, pp. 184-197 in McNiven, D., ed., *Moral expertise: Studies in practical and professional ethics*,
371 Routledge: London & New York.
- 372 McKay, C.P., Toon, O.B. and Kasting, J.F., 1991. Making Mars habitable. *Nature*, 352(6335), pp.489-496.
- 373 MEPAG, Mars Scientific Goals, Objectives, Investigations, and Priorities: 2025. D. Banfield, ed., 78 p.
374 white paper posted September, 2025 by the Mars Exploration Program Analysis Group (MEPAG) at
375 <https://www.lpi.usra.edu/mepag/goals/>
- 376 Mischna, M.A., Allen, M., Richardson, M.I., Newman, C.E. and Toigo, A.D., 2011. Atmospheric modeling
377 of Mars methane surface releases. *Planet. Space Sci.*, 59(2-3), pp.227-237.
378 <https://doi.org/10.1016/j.pss.2010.07.005>
- 379 Montabone, L., Forget, F., Millour, E., Wilson, R.J., Lewis, S.R., Cantor, B., Kass D., et al., 2015. Eight-
380 year climatology of dust optical depth on Mars. *Icarus*, 251: 65-95.
381 <https://doi.org/10.1016/j.icarus.2014.12.034>
- 382 Murphy, J.R., Haberle, R.M., Toon, O.B., & Pollack, J.B., 1993. Martian global dust storms: Zonally
383 symmetric numerical simulations including size-dependent particle transport. *J. Geophys. Res.:
384 Planets*, 98(E2), 3197-3220. <https://doi.org/10.1029/92JE02945>
- 385 Newman, C.E., Lewis, S.R., Read, P.L., and Forget, F., 2002. Modeling the Martian dust cycle 2.
386 Multiannual radiatively active dust transport simulations. *J. Geophys. Res.: Planets* 107, E12, 7-1.
387 <https://doi.org/10.1029/2002JE001920>
- 388 Ohneiser, K., Ansmann, A., Witthuhn, J., Deneke, H., Chudnovsky, A., Walter, G. and Senf, F., 2023. Self-
389 lofting of wildfire smoke in the troposphere and stratosphere: simulations and space lidar
390 observations. *Atmospheric Chemistry and Physics*, 23(4), pp.2901-2925. [https://doi.org/10.5194/acp-23-
391 2901-2023](https://doi.org/10.5194/acp-23-2901-2023)
- 392 Pollack, J.B., and Sagan, C., Planetary engineering, p.921-950 in Lewis, J.S., Matthews, M.S. and Guerrieri,
393 M.L., 1993. *Resources of Near-Earth Space*, University of Arizona Press.

- 394 Rafkin, S.C., 2009. A positive radiative-dynamic feedback mechanism for the maintenance and growth of
 395 Martian dust storms. *J. Geophys. Res.: Planets*, 114(E1). <https://doi.org/10.1029/2008JE003217>
- 396 Ramirez, R.M., 2017. A warmer and wetter solution for early Mars and the challenges with transient
 397 warming. *Icarus*, 297, pp.71-82. <https://doi.org/10.1016/j.icarus.2017.06.025>
- 398 Richardson, M.I., & Kite, E.S. (2025). Supplementary data for "Atmospheric dynamics of first steps toward
 399 terraforming Mars", by Richardson et al. [Data set]. Zenodo. <https://doi.org/10.5281/zenodo.17844025>
- 400 Richardson, M.I. and Wilson, R.J., 2002. A topographically forced asymmetry in the Martian circulation
 401 and climate. *Nature*, 416(6878), pp.298-301. <https://doi.org/10.1038/416298a>
- 402 Richardson, M.I., Toigo, A.D. and Newman, C.E., 2007. PlanetWRF: A general purpose, local to global
 403 numerical model for planetary atmospheric and climate dynamics. *J. Geophys. Res.: Planets*, 112(E9).
 404 <https://doi.org/10.1029/2006JE002825>
- 405 Sagan, C., 1973, Planetary engineering on Mars. *Icarus* 20, no. 4: 513-514. <https://doi.org/10.1016/0019->
 406 [1035\(73\)90026-2](https://doi.org/10.1016/0019-1035(73)90026-2)
- 407 Spiga, A., Faure, J., Madeleine, J.B., Määttänen, A. and Forget, F., 2013. Rocket dust storms and detached
 408 dust layers in the Martian atmosphere. *J. Geophys Res: Planets*, 118(4), pp.746-767.
 409 <https://doi.org/10.1002/jgre.20046>
- 410 Stern, J.C., Malespin, C.A., Eigenbrode, J.L., Webster, C.R., Flesch, G., Franz, H.B., Graham, H.V., House,
 411 C.H., Sutter, B., Archer, Jr, P.D. and Hofmann, A.E., 2022. Organic carbon concentrations in 3.5-billion-
 412 year-old lacustrine mudstones of Mars. *Proc. Nat. Acad. Sci.*, 119(27), p.e2201139119.
 413 <https://doi.org/10.1073/pnas.220113911>
- 414 Toigo, A.D., Lee, C., Newman, C.E. and Richardson, M.I., 2012. The impact of resolution on the dynamics
 415 of the Martian global atmosphere: Varying resolution studies with the MarsWRF GCM. *Icarus*, 221(1),
 416 pp.276-288. <https://doi.org/10.1016/j.icarus.2012.07.020>
- 417 Urata, R.A., Bertrand, T., Kahre, M.A., Wilson, R.J., Kling, A.M. and Wolff, M., 2025. Impact of a bimodal
 418 dust distribution on the 2018 Martian global dust storm with the NASA Ames Mars global climate model.
 419 *Icarus*, 429, p.116446. <https://doi.org/10.1016/j.icarus.2024.116446>
- 420 Visioni, D., MacMartin, D.G., Kravitz, B., Lee, W., Simpson, I.R. and Richter, J.H., 2020. Reduced
 421 poleward transport due to stratospheric heating under stratospheric aerosols geoengineering. *Geophys. Res.*
 422 *Let.*, 47(17), p.e2020GL089470. <https://doi.org/10.1029/2020GL089470>
- 423 Wilson, R.J., & Hamilton, K., 1996. Comprehensive model simulation of thermal tides in the Martian
 424 atmosphere. *J. Atmos. Sci.*, 53(9), 1290-1326. <https://doi.org/10.1175/1520->
 425 [0469\(1996\)053<1290:CMSOTT>2.0.CO;2](https://doi.org/10.1175/1520-0469(1996)053<1290:CMSOTT>2.0.CO;2)

426 Wilson, R.J., Lewis, S.R., Montabone, L., & Smith, M.D., 2008. Influence of water ice clouds on Martian
427 tropical atmospheric temperatures. *Geophys. Res. Lett.*, 35(7).

428 <https://doi.org/10.1029/2007GL032405>

429 Wordsworth, R., Kerber, L. and Cockell, C., 2019. Enabling Martian habitability with silica aerogel via the
430 solid-state greenhouse effect. *Nature Astronomy*, 3(10), pp.898-903. [https://doi.org/10.1038/s41550-019-](https://doi.org/10.1038/s41550-019-0813-0)
431 0813-0

432 Wordsworth, R. and Cockell, C., 2024. Self-sustaining living habitats in extraterrestrial
433 environments. *Astrobiology*, 24(12), pp.1187-1195. <https://doi.org/10.1089/ast.2024.0080>

434 Wordsworth, R., Cherubim, C., Nangle, S., Berliner, A., Dyson, E., Girguis, P., Grinspoon, D., Harris, R.,
435 Liu, K., Marblestone, A. and Mason, C., 2025. Applied astrobiology: An integrated approach to the future
436 of life in space. *Astrobiology* 25(5), 327-330. <https://doi.org/10.1089/ast.2024.0156>

437 Xia, Y., Hu, Y. and Liu, J., 2020. Comparison of trends in the Hadley circulation between CMIP6 and
438 CMIP5. *Science Bulletin*, 65(19), pp.1667-1674. <https://doi.org/10.1016/j.scib.2020.06.011>

439 Yu, P., Toon, O.B., Bardeen, C.G., Zhu, Y., Rosenlof, K.H., Portmann, R.W., Thornberry, T.D., Gao, R.S.,
440 Davis, S.M., Wolf, E.T. and de Gouw, J., 2019. Black carbon lofts wildfire smoke high into the stratosphere
441 to form a persistent plume. *Science*, 365(6453), pp.587-590. DOI: 10.1126/science.aax1748

442 Yung, Y.L. and DeMore, W.B., 1999. *Photochemistry of Planetary Atmospheres*. Oxford University Press.

443 Zhang, J. and Shao, Y., 2014. A new parameterization of particle dry deposition over rough surfaces.
444 *Atmospheric Chemistry and Physics*, 14(22), pp.12429-12440. <https://doi.org/10.5194/acp-14-12429-2014>

445

446 **Supporting References.**

447 Bertrand, T., Kahre, M.A., Urata, R., Määttänen, A., Montmessin, F., Wilson, R.J., and Wolff, M.J.,
448 2022. Impact of the coagulation of dust particles on Mars during the 2018 global dust storm. *Icarus*, 388,
449 p.115239. <https://doi.org/10.1016/j.icarus.2022.115239>

450 Deokar, G., Jin, J., Schwingenschlögl, U., Kanoun, M.B., and Costa, P.M.F.J., 2022. Chemical vapor
451 deposition-grown nitrogen-doped graphene's synthesis, characterization and applications. *npj 2D Mater*
452 *Appl*, 6, p.14. <https://doi.org/10.1038/s41699-022-00287-8>

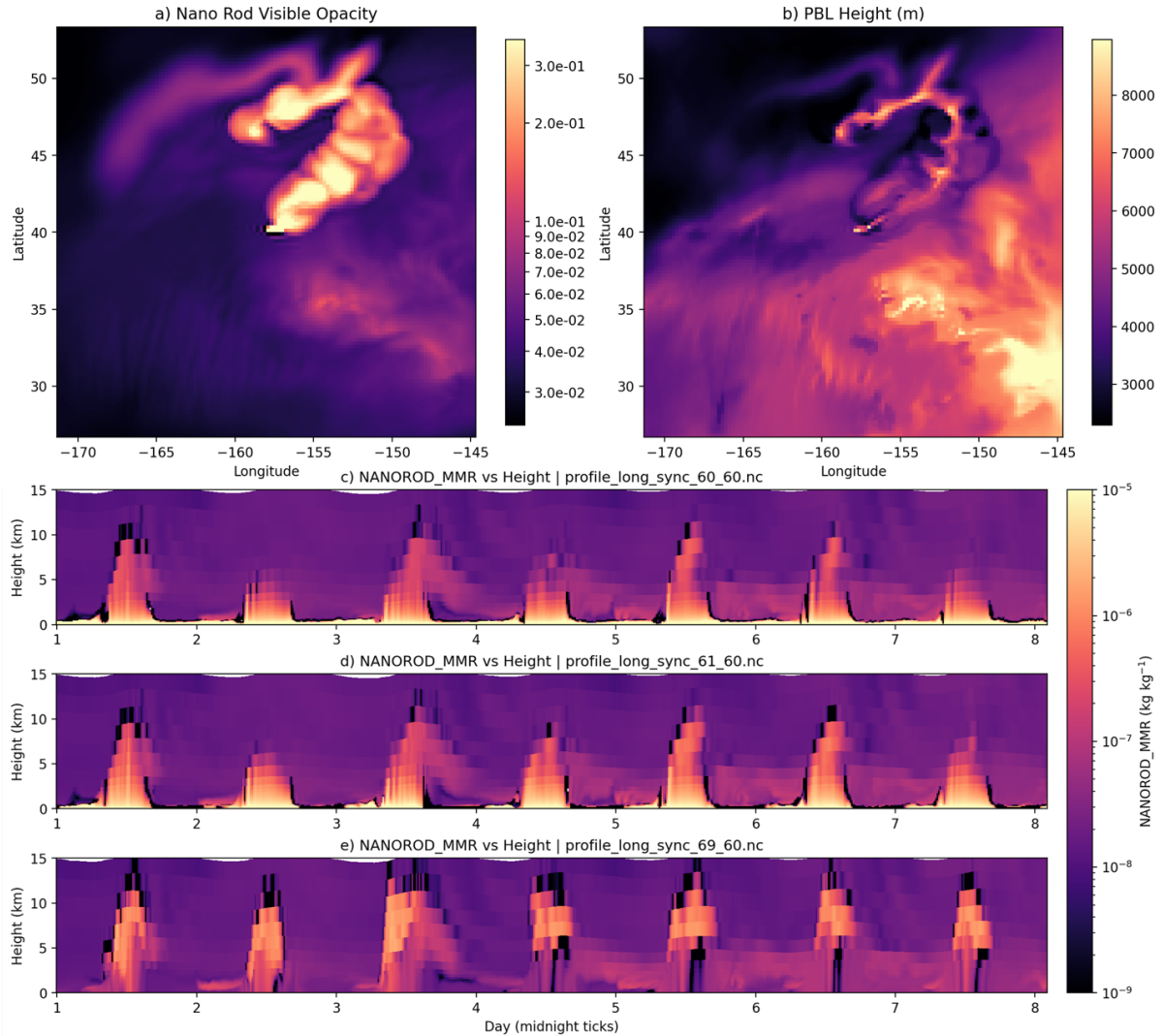
453 Grebenko, A.K., Krasnikov, D.V., Bubis, A.V., Stolyarov, V.S., Vyalikh, D.V., Makarova, A.A.,
454 Fedorov, A., Aitkulova, A., Alekseeva, A.A., Gilshtein, E., and Bedran, Z., 2022. High-quality graphene
455 using Boudouard reaction. *Advanced Science*, 9(12), p.2200217. <https://doi.org/10.1002/advs.202200217>

456 Guo, B., Fang, L., Zhang, B., and Gong, J.R., 2011. Graphene doping: a review. *Insciences J.*, 1(2),
457 pp.80-89. <https://doi.org/10.5640/insc.010280>

- 458 Haberle, R.M., 2013. Estimating the power of Mars' greenhouse effect. *Icarus*, 223(1), pp.619-620.
 459 <https://doi.org/10.1016/j.icarus.2012.12.022>
- 460 Haberle, R.M., Clancy, R.T., Forget, F., Smith, M.D., and Zurek, R.W. eds., 2017. *The Atmosphere and*
 461 *Climate of Mars*. Cambridge University Press.
- 462 Haberle, R.M., Kahre, M.A., Bertrand, T., and Wolff, M.J., 2025. Modeling studies of dust/gas non-
 463 thermal equilibrium in the Martian atmosphere. *Icarus*, 429, p.116452.
 464 <https://doi.org/10.1016/j.icarus.2024.116452>
- 465 Hartwick, V.L., Haberle, R.M., Kahre, M.A., and Wilson, R.J., 2022. The dust cycle on Mars at different
 466 orbital distances from the Sun: An investigation of the impact of radiatively active dust on land planet
 467 climate. *Astrophysical Journal*, 941(1), p.54. <https://doi.org/10.3847/1538-4357/ac9481>
- 468 Hartwick, V.L., Toon, O.B., Lundquist, J.K., Pierpaoli, O.A., and Kahre, M.A., 2023. Assessment of
 469 wind energy resource potential for future human missions to Mars. *Nature Astronomy*, 7(3), pp.298-308.
 470 <https://doi.org/10.1038/s41550-022-01851-4>
- 471 He, C., Jiang, S., and Shen, P., 2013. Large-scale and rapid synthesis of disk-shaped and nano-sized
 472 graphene. *Scientific Reports*, 3, p.2144. <https://doi.org/10.1038/srep02144>
- 473 Hinterman, E.D., 2022. Multi-objective system optimization of a Mars atmospheric ISRU plant (Doctoral
 474 dissertation, Massachusetts Institute of Technology), <https://hdl.handle.net/1721.1/145095>
- 475 Hoffman, J.A., Hecht, M.H., Rapp, D., Hartvigsen, J.J., SooHoo, J.G., Aboobaker, A.M., McClean, J.B.,
 476 Liu, A.M., Hinterman, E.D., Nasr, M., and Hariharan, S., 2022. Mars Oxygen ISRU Experiment
 477 (MOXIE)—preparing for human Mars exploration. *Science Advances*, 8(35), p.eabp8636.
 478 <https://doi.org/10.1126/sciadv.abp8636>
- 479 Hong, S. Y., Noh, Y., and Dudhia, J. (2006). A new vertical diffusion package with an explicit treatment
 480 of entrainment processes. *Monthly Weather Review*, 134(9), 2318-2341.
 481 <https://doi.org/10.1175/MWR3199.1>
- 482 Klimchitskaya, G.L., and Mostepanenko, V.M., 2013. Van der Waals and Casimir interactions between
 483 two graphene sheets. *Physical Review B---Condensed Matter and Materials Physics*, 87(7), p.075439.
 484 <https://doi.org/10.1103/PhysRevB.87.075439>
- 485 Li, L., Zhao, C., Newman, C. E., Zhao, Y., Feng, J., Li, T., et al. (2025). Impacts of dry deposition
 486 processes with resolved dust particle sizes on simulating the Martian dust. *Journal of Geophysical*
 487 *Research: Planets*, 130, e2024JE008616. <https://doi.org/10.1029/2024JE008616>
- 488 Liu, H., Liu, Y., and Zhu, D., 2010. Chemical doping of graphene. *J. Mater. Chem.*, 20, pp.10928-10934.
- 489 Luong, D.X., Bets, K.V., Algozeeb, W.A., Stanford, M.G., Kittrell, C., Chen, W., Salvatierra, R.V., Ren,
 490 M., McHugh, E.A., Advincula, P.A., and Wang, Z., 2020. Gram-scale bottom-up flash graphene
 491 synthesis. *Nature*, 577(7792), pp.647-651. <https://doi.org/10.1038/s41586-020-1938-0>

- 492 Madeleine, J.B., Head, J.W., Forget, F., Navarro, T., Millour, E., Spiga, A., Colaëtis, A., Määttänen, A.,
 493 Montmessin, F., and Dickson, J.L., 2014. Recent ice ages on Mars: The role of radiatively active clouds
 494 and cloud microphysics. *Geophys. Res. Lett.*, 41(14), pp.4873-4879.
 495 <https://doi.org/10.1002/2014GL059861>
- 496 Manabe, S., and Wetherald, R.T., 1967. Thermal equilibrium of the atmosphere with a given distribution
 497 of relative humidity. *J. Atmos. Sci.*, 24, pp.241-259. [https://doi.org/10.1175/1520-0469\(1967\)024<0241:TEOTAW>2.0.CO;2](https://doi.org/10.1175/1520-0469(1967)024<0241:TEOTAW>2.0.CO;2)
- 499 Mbayachi, V.B., Ndayiragije, E., Sammani, T., Taj, S., Mbuta, E.R., and Khan, A.U., 2021. Graphene
 500 synthesis, characterization and its applications: A review. *Results in Chemistry*, 3, p.100163.
 501 <https://doi.org/10.1016/j.rechem.2021.100163>
- 502 McClellan, J., Keith, D.W., and Apt, J., 2012. Cost analysis of stratospheric albedo modification delivery
 503 systems. *Environ. Res. Lett.*, 7(3), p.034019. <https://doi.org/10.1088/1748-9326/7/3/034019>
- 504 Mischna, M.A., Lee, C., and Richardson, M., 2012. Development of a fast, accurate radiative transfer
 505 model for the Martian atmosphere, past and present. *J. Geophys. Res.: Planets*, 117(E10).
 506 <https://doi.org/10.1029/2012JE004110>
- 507 Neto, A.H., Guinea, F., Peres, N.M.R., Novoselov, K.S., and Geim, A.K., 2009. The electronic properties
 508 of graphene. *Rev. Mod. Phys.*, 81, pp.109-162. <https://doi.org/10.1103/RevModPhys.81.109>
- 509 Paton, K.R., Varrla, E., Backes, C., Smith, R.J., Khan, U., O'Neill, A., Boland, C., Lotya, M., Istrate,
 510 O.M., King, P., and Higgins, T., 2014. Scalable production of large quantities of defect-free few-layer
 511 graphene by shear exfoliation in liquids. *Nature Materials*, 13(6), pp.624-630.
 512 <https://doi.org/10.1038/nmat3944>
- 513 Rakić, A.D., 1995. Algorithm for the determination of intrinsic optical constants of metal films:
 514 Application to aluminum. *Applied Optics*, 34, pp.4755-4767. <https://doi.org/10.1364/AO.34.004755>
- 515 Ramirez, R.M., and Kasting, J.F., 2017. Could cirrus clouds have warmed early Mars? *Icarus*, 281,
 516 pp.248-261. <https://doi.org/10.1016/j.icarus.2016.08.016>
- 517 Ramirez, R.M., Kopparapu, R., Zuger, M.E., Robinson, T.D., Freedman, R., and Kasting, J.F., 2014.
 518 Warming early Mars with CO₂ and H₂. *Nat. Geosci.*, 7, pp.59-63. <https://doi.org/10.1038/ngeo2000>
- 519 Rapp, D., and Hinterman, E., 2023. Adapting a Mars ISRU System to the Changing Mars Environment.
 520 *Space: Science & Technology*, 3, p.0041. <https://doi.org/10.34133/space.0041>
- 521 Sharipov, F., *Rarefied Gas Dynamics: Fundamentals for Research and Practice* (Wiley-VCH, Berlin,
 522 2016).
- 523 Romero-Guzman, C., Perez-Grande, I. and Rodriguez-Manfredi, J.A., 2023. Thermal model of InSight
 524 solar panels in Martian conditions. *Acta Astronautica*, 202, pp.476-484.

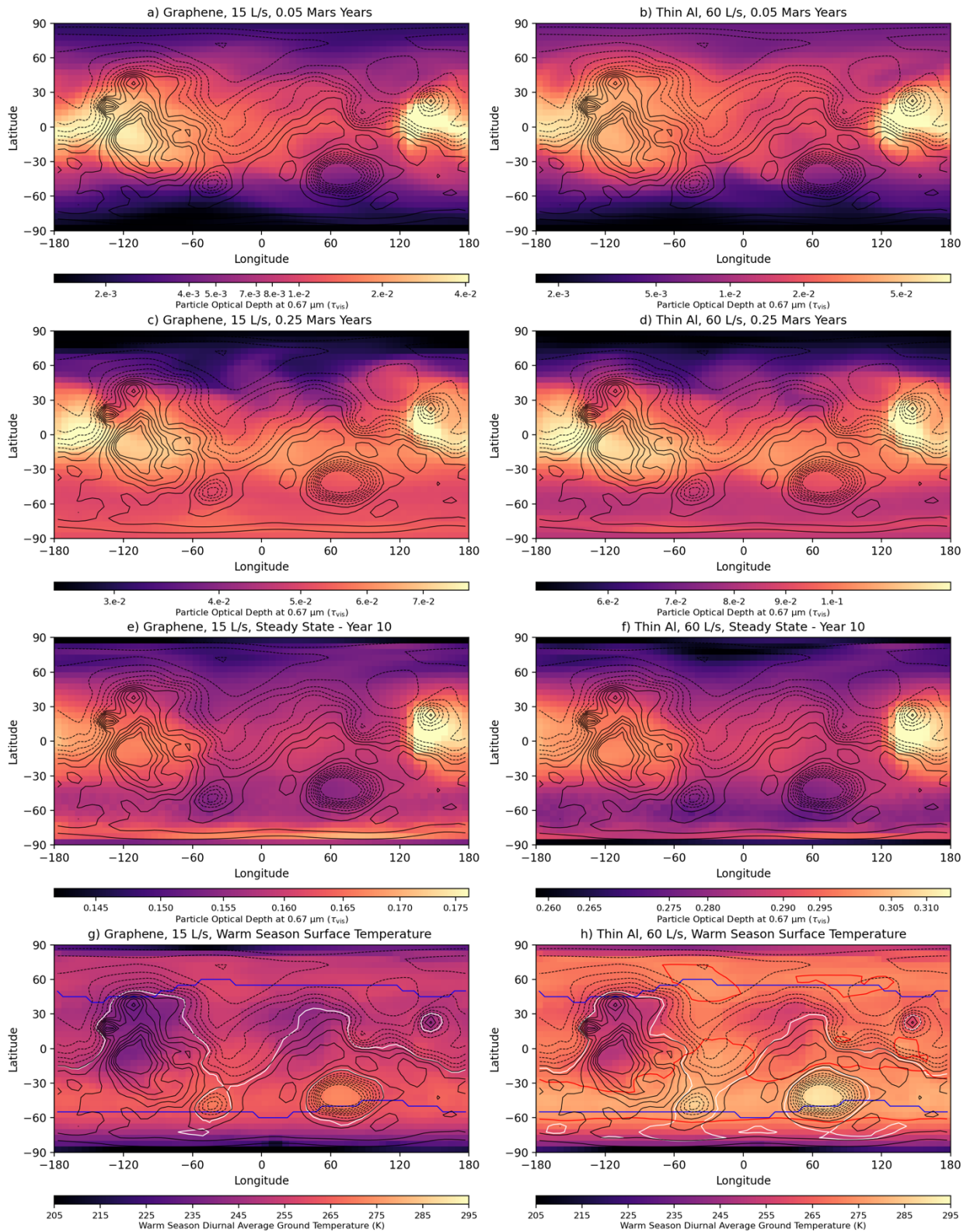
- 525 Staley, J.T., and Haupin, W., 2000, Aluminum and aluminum alloys, in *Kirk-Othmer Encyclopedia of*
526 *Chemical Technology*, 4th Edition, volume 2, Kirk-Othmer.
- 527 Streeter, P.M., Lewis, S.R., Patel, M.R., Holmes, J.A., and Kass, D.M., 2020, Surface warming during the
528 2018/Mars year 34 global dust storm. *Geophys. Res. Lett.* 47, e2019GL083936.
529 <https://doi.org/10.1029/2019GL083936>
- 530 Thekaekara, M.P., 1973. Solar energy outside the Earth's atmosphere. *Solar Energy*, 14, pp.109-127.
531 [https://doi.org/10.1016/0038-092X\(73\)90028-5](https://doi.org/10.1016/0038-092X(73)90028-5)
- 532 Tikuišis, K.K., Dubroka, A., Uhlířová, K., Speck, F., Seyller, T., Losurdo, M., Orlita, M., and Veis, M.,
533 2023. Dielectric function of epitaxial quasi-freestanding monolayer graphene on Si-face 6H-SiC in a
534 broad spectral range. *Phys. Rev. Materials*, 7, p.044201.
535 <https://doi.org/10.1103/PhysRevMaterials.7.044201>
- 536 Williams, R.J., McKay, D.S., Giles, D., and Bunch, T.E., 1979. Mining and beneficiation of lunar ores.
537 *Space Resources and Space Settlements* (NASA SP-428), pp.275-188.
- 538 Wollman, M.J., and Zika, M.J. Prometheus Project Reactor Module Final Report, For Naval Reactors
539 Information, Apr. 2006. <https://doi.org/10.2172/884680>



540

Fig. 1. Local plume dynamics during initial deployment of 60 nm diameter Al rods at 60 L/s. Results are captured ~6 sols from the time the plume is initiated. **(a)** Column-integrated opacity of particle plume at wavelength = 0.67 μm (τ_{vis} , unitless). **(b)** Planetary boundary layer (PBL) height (m). Both panels are for the same timestep, with a true local solar time of 11AM at the source site. A mix of shadowing of the ground by plume particles and radiative heating of plume particles leads to a mixture of PBL suppression and augmentation in different locations. **(c-e)** Time-height cross-sections of plume mass mixing ratio in the lowest 10 km. **(c)** is centered over the plume release site, **(d)** is one grid point (~10 km) to the east, and **(e)** is ~100 km further east. Nighttime accumulation in the stable surface layer is evident as a lighter color / yellow band; daytime convection ventilates the accumulated particles deep into the atmosphere, which can then advect downwind in the free atmosphere. Results are for release at Arcadia Planitia (202°E 40°N). MarsWRF has been set up to nest from 2°×2° GCM domain, with two levels of nesting. The nested domain shown has 120×120 grid points and a grid spacing of 0.222°, corresponding to less than 13 km.

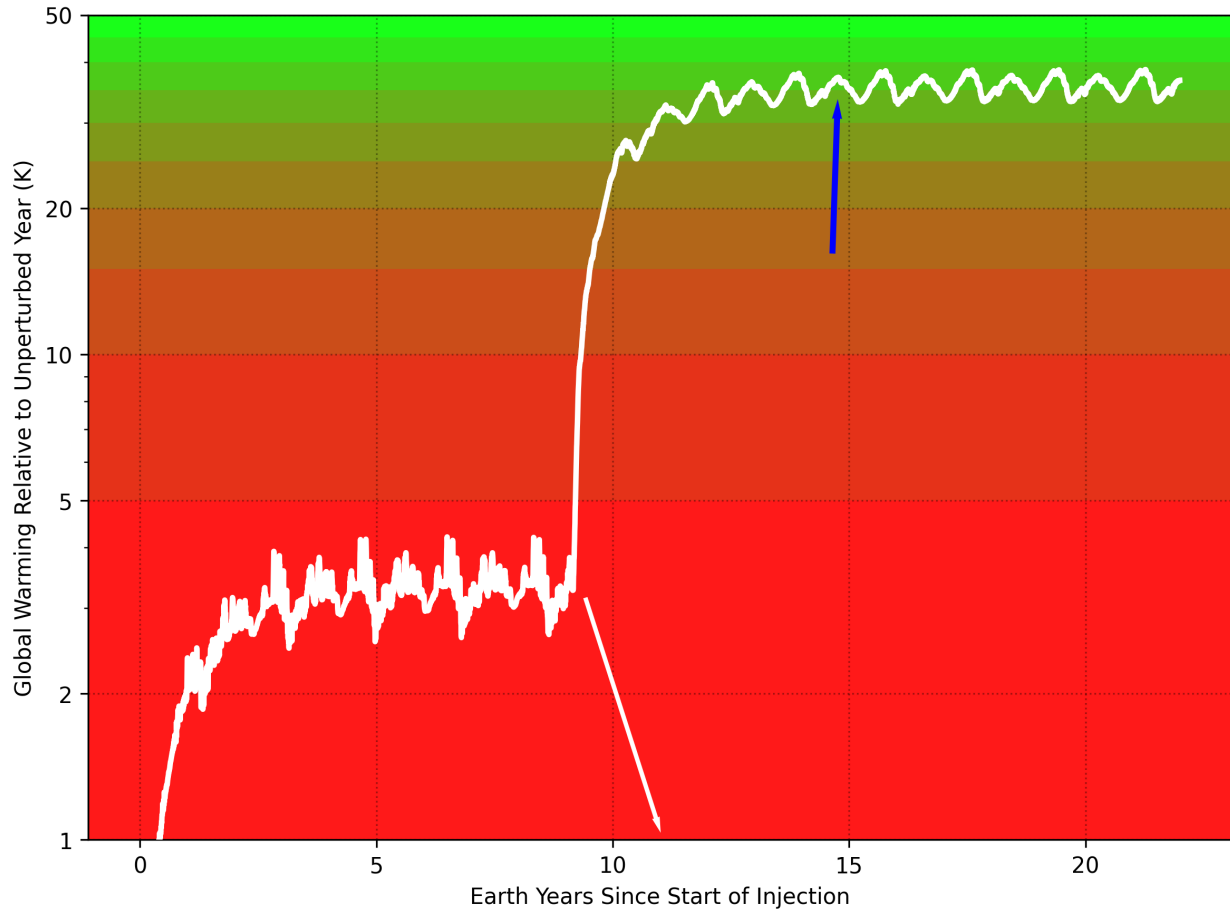
541



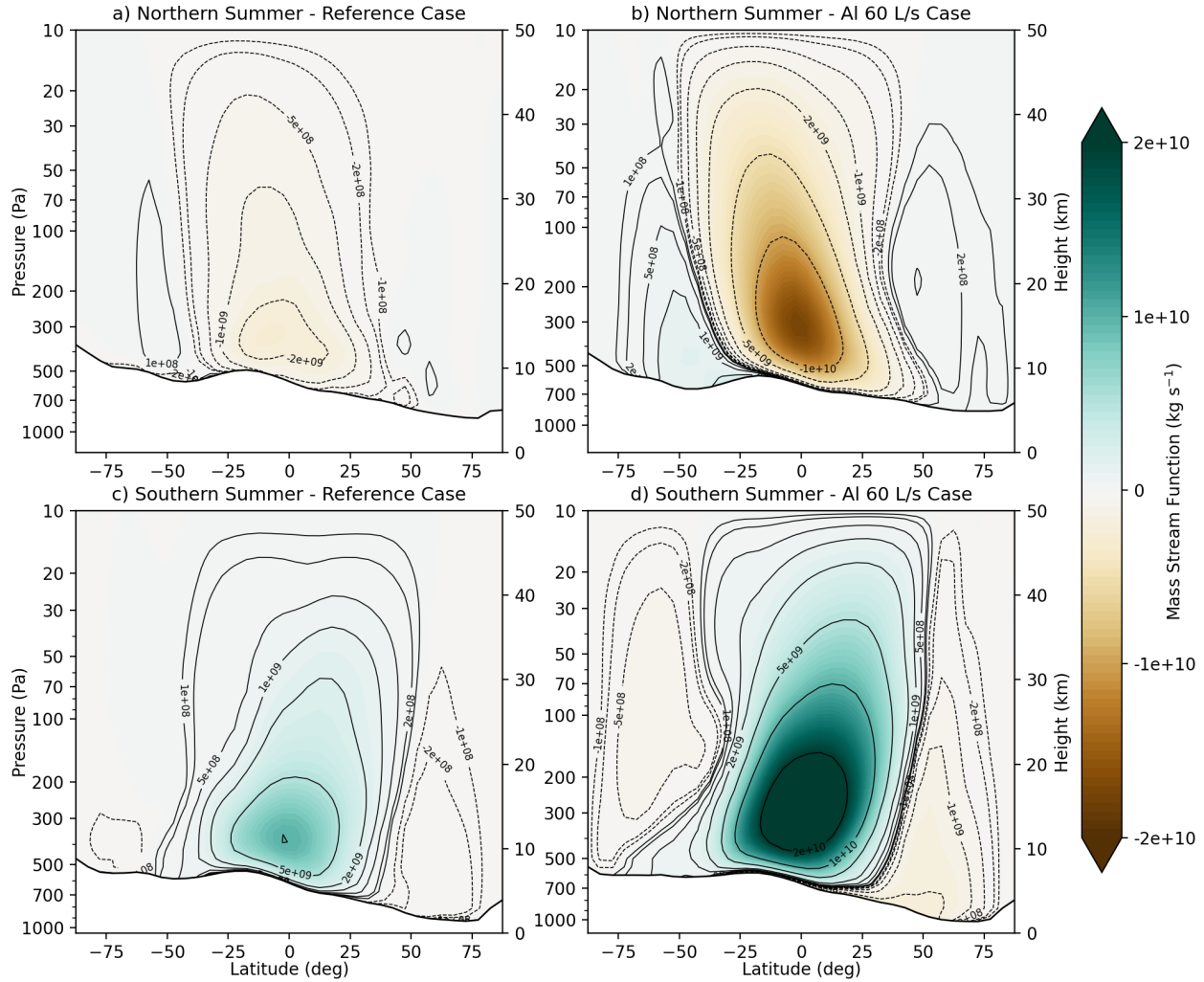
542

Fig. 2. Dynamics of particle spread and steady-state global warming. Left: 15 L/s carbon (graphene) disks (*run Cc41*). Right: 60 L/s metal rods (*run Cc16*). Both assuming 0°N 135°E release. **(a-f)** Particle optical depth at 0.67 μm (τ_{vis}). **(g and h)** Filled color: warm season temperatures (K). Black topographic contours correspond to elevations of -5 and -2 km (dashed), and 0, +2, and +5 km (solid). White contour: 610 Pa (~6 mbar) mean pressure level. Blue contour: Approximate equatorward extent of H₂O ice at <1 m depth based on GRS data (Feldman *et al.*, 2004). Red contour: Highlights warm-season average surface temperatures above 273K.

543



544 **Fig. 3.** Time evolution of global average surface temperature, assuming a 3 L/s IR-active particle
 545 release starting at the northern equinox for the first 5 Mars years (just over 9 Earth years), followed
 546 by increase to 60 L/s. All particles assumed. These two different rates show that the response
 547 timescale is almost independent of the release rate. After 8 Mars years (15 Earth-yr, indicated by
 548 blue arrow), the average warm-season temperature at 47.5°S exceeds 280 K. The line is
 549 constructed by taking the daily global average surface temperature and removing from it the global
 550 average temperature for the same day-of-year (sol) from the steady-state reference run. Note that
 551 net warming is a modest function of season due to the distribution of nanoparticles. If a choice is
 552 made to cease warming, then the planet rapidly cools to the no-warming state (roughly following
 553 the white arrow to zero warming).



554

555 **Fig. 4. Atmospheric circulation strengthens under aerosol warming.** Streamfunctions (kg/s)
 556 for (a, c) control and (b, d) 60 L/s Al-particle warming cases. (a-b) Northern summer, (c-d)
 557 southern summer. Positive values: clockwise mass flux (looking toward the west). The surface
 558 pressure changes due to the reduction in seasonal CO₂ ice in the warmed case. Note that the plot
 559 is limited to 50 km to focus on the lower-to-mid tropospheric circulation, but the model top is at
 560 roughly 100 km.